UNIVERSITY OF CALIFORNIA
RIVERSIDE

Sensitivity Study of a High Aspect-Ratio Flow Diverter for Cerebral Aneurysms

A Thesis submitted in partial satisfaction
of the requirements for the degree of

Master of Science

in

Mechanical Engineering

by

Edver Bahena

December 2019

Thesis Committee:

Dr. Masaru P. Rao, Chairperson
Dr. Monica Martinez
Dr. Guillermo Aguilar

The Thesis of Edver Bahena is approved:

_____

_____

_____

Committee Chairperson

University of California, Riverside

Acknowledgments

I'd like to thank my PI Dr. Masaru Rao for the opportunity of becoming a member of his research lab. In these past few years I have gained valuable experiences and skills as a researcher. Your constant support and encouragement is deeply appreciated by me and the lab. Also, I'd like to thank Dr. Monica Martinez Wilhelmus for your expertise in PIV, our group advanced significantly with your help.

This work would have not been possible without the support of the Biomedical Microdevices Laboratory group. A big thanks to Dr. Bryan Woo, Dr. Harish Dixit, Dr. Duncan Ashby, Benjamin Sommerkorn, Samantha Corber, Kairui Xia, Sanika Nishandar, and Morgan Dundon for always willing to act as consultants whenever the research got tough. I owe a special thanks to my senior labmate, Ryan Peck. It was a pleasure to work with you on this research project, and I appreciate the time you took to help me get up to speed.

I also would like to thank my parents, Maria and Pedro Bahena for the constant support and encouragement in my academic journey. Through your hard work and sacrifices you showed me that I could achieve anything. I hope that I have made you two proud. My brother, Edwin Bahena, thank you for the constant source laughter and encouragement during all the late nights I had while working on this project.

Lastly, I would like to thank my girlfriend, Jacqueline Mantooth. Words can't describe the amount of gratitude I have for you. Thank you for the constant support and for always reassuring me that I was capable of completing this work. I hope that I can do the same for you in whatever projects you choose to take on in life.

ABSTRACT OF THE THESIS

Sensitivity Study of a High Aspect-Ratio Flow Diverter for Cerebral Aneurysms

by

Edver Bahena

Master of Science, Graduate Program in Mechanical Engineering
University of California, Riverside, December 2019
Dr. Masaru P. Rao, Chairperson

Stroke is the fourth leading cause of death in the United States with a high morbidity rate for both ischemic and hemorrhagic strokes. Although the majority of stokes that occur are ischemic, these patients have a high chance of survivability if treated. However, 50% of patients with hemorrhagic stroke, prognosis of death within the first six months is high. Hemorrhagic strokes typically occur due to rupture of an intracerebral aneurysm (i.e., a portion of a neurovasculature that has ballooned out due to disease-induced weakening). Current treatment methods are moving toward less invasive techniques to treat aneurysms before rupture occurs, one particularly compelling example of which is the flow diverter (FDs). These devices redirect flow away from the aneurysm sac, and they have been shown to allow for healing of the diseased tissue. Flow diverters are currently fabricated by braiding individual wires into a mesh-like structure. However, due to this design, coupled with the typical location of the aneurysms being treated, there is a high chance of occluding small perforator arteries as well. Our lab is developing a new concept for FD design, enabled by novel MEMS fabrication techniques we have pioneered, which seeks to

address this limitation via use of high-aspect-ratio (height-to-width ratio) struts. The study described herein, has sought to explore the effect of device placement and strut thickness on flow diversion performance within this context.

Table of Contents

TABLE OF FIGURES

1. INTRODUCTION

1.1 Background

Recent research has shown that strokes remain the fourth leading cause of death in the United States (Benjamin et al., 2019). There are two types of strokes, ischemic and hemorrhagic. About 87% of all stokes are ischemic with 13% of them being hemorrhagic strokes (Demaerschalk et al., 2010). Ischemic strokes are the result of blockage to an artery in the brain, thus reducing blood flow and nutrient transport. If patients receive drugs that promote thrombolysis within three hours of incidence, survivability increases to 30% (Novakovic et al., 2009). Although most stroke patients have an ischemic stroke, hemorrhagic stroke survivability in patients is much less. A hemorrhagic stroke happens when an already weakened blood vessel wall ruptures and allows blood to flow into the intracranial space. This is initially caused by vessel wall weakness which manifests itself as the formation of an aneurysm. This balloon-like structure is the initial angiographic indication of an increased risk of hemorrhagic stroke as shown in Figure 1. Approximately 6 million Americans are afflicted with an unruptured cerebral aneurysm, and while normally harmless, 25% of ruptures lead to death in the first 24 hours and another 25% will die within the first six months (NIND, 2018).

Direct surgical approaches to aneurysm treatments are becoming utilized less often because of the high incidence of morbidity as a result of surgical complications. With current treatment methods moving towards noninvasive techniques for preventing aneurysm rupture, the need for next generation devices is rapidly increasing. There are several types of treatment options such as clipping the aneurysm, filling the aneurysm sac with a coil, or divert flow away from the aneurysm using a flow diverter. Currently only

one flow diverting device, Pipeline Embolization Device (PED), has been approved by the FDA for use in the anterior region of the brain. Herein we demonstrate a new novel device that can be used for the posterior circulation that overcomes the current limitations of Pipeline. Some of the limitations of Pipeline include occlusion of perforators and the wide variability of porosity when deployed in the parent artery.

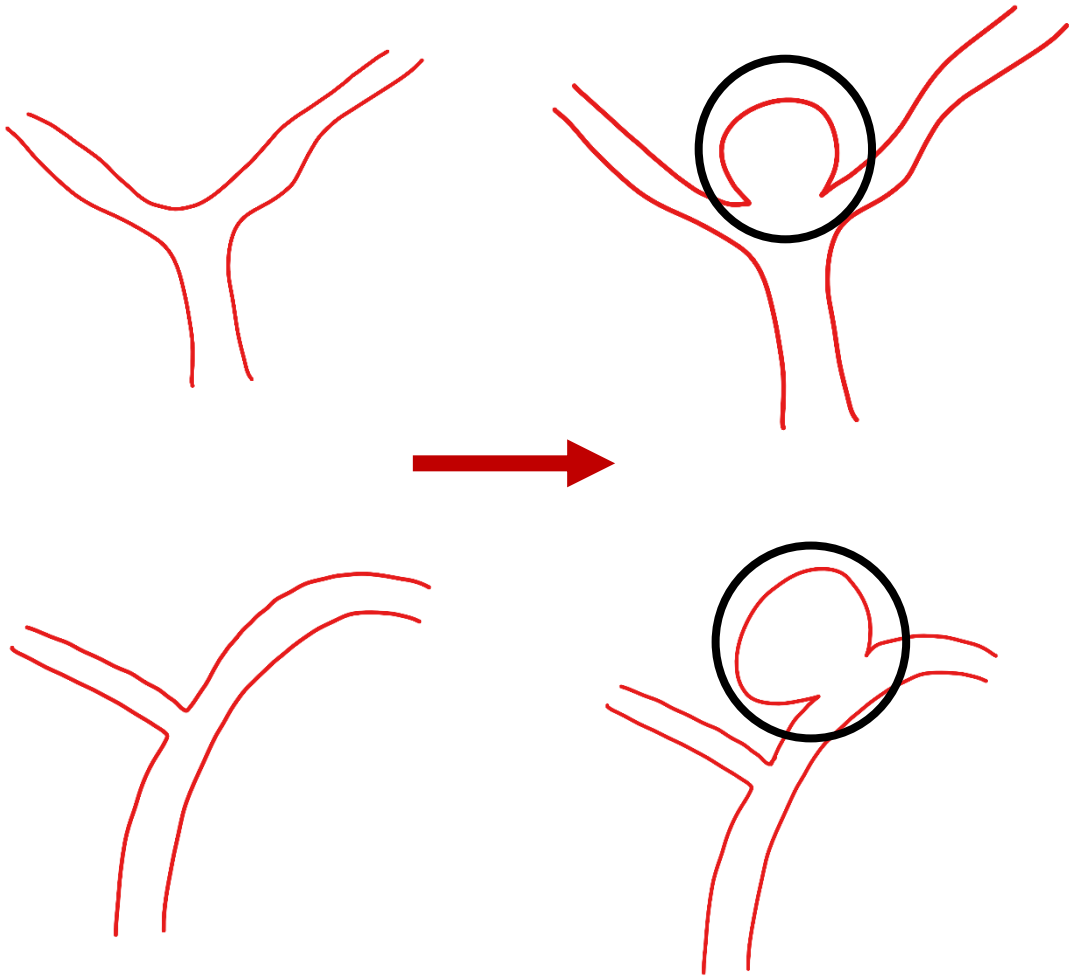

Figure 1: Shown from left to right, a healthy blood vessel with no aneurysm to a diseased blood vessel with a saccular aneurysm.

1.2 Aneurysm Morphology

There are two types of aneurysm morphologies, fusiform and saccular. Fusiform aneurysms are an expansion of the artery along its wall leading to a widening of the artery. Saccular aneurysm, also called berry aneurysms, which account for 90% of cerebral aneurysms, form when a portion of the artery wall expands outward into a balloon shape.

About 85% of cerebral aneurysms occur in a portion of the brain vasculature called the Circle of Willis (Keedy, 2006). The Circle of Willis is a connective network of blood vessels at the base of the brain. It's been observed that morphological changes or asymmetries of the full Circle of Willis highly correlate with the presence of aneurysms (Stojanović et al. 2006) . However, it is not yet fully established as to why this happens. It is hypothesized that the imbalances in blood flow or pressure in certain parts of the circle of Willis due to asymmetry could lead to aneurysm formation.

The magnitude of the pressure observed gives an insight into the forces that are exerted onto the vessel walls. Both the magnitude and the directionality of the velocity of blood flow, are important characteristics to note during aneurysm formation. If the endothelial lining experiences flows that do not align parallel with the endothelial cells' growth direction and/or experiences high flows that continually hit a specific portion of the vascular wall, an aneurysm might develop over time due to the weakening in the endothelium. Additionally, the direction of blood flow can have implications for chemical signaling negatively affecting endothelial cell growth. Endothelial cells require both a chemical and mechanical stimulus to stay healthy and both factors are greatly affected by the development of an aneurysm.

1.3 Treatments

1.3.1 Clipping

The historic and most established way of treating an aneurysm has been surgical clipping. Surgical clipping has been used since the late 1930's and is considered the gold standard for treating aneurysms. Clipping is achieved by the patients undergoing a craniotomy, where a small portion of the skull is removed allowing the surgeon to place a small clip around the neck of the aneurysm (Dandy, 1938). While clipping was one of the first methods used to treat aneurysms, it is highly invasive and can lead to further complications after surgery such as subarachnoid hemorrhaging. With improvements in surgery technology, the surgical morbidity of craniotomies has decreased, however the surgery remains highly invasive. This has the effect of excluding a large segment of the stroke patient population who often have other comorbidities which further complicate recovery and render the surgical risk unacceptable.

1.3.2 Endovascular Coiling

Another method currently used for treating aneurysms is coiling. This method uses a metal wire that is guided into the aneurysm sac using a catheter, which is inserted through the femoral artery and guided to the aorta which allows it to be further guided up to the brain vasculature. Once the catheter reaches the aneurysm location, a metal wire is deployed and is wound inside the sac essentially blocking any blood flow from entering. One drawback of this method is that it is limited to aneurysm sacs with small neck openings. Small neck openings are needed to keep the coil wound up inside the sac and to prevent the coil from

escaping. There have also been reports of the coil becoming unwound and rupturing the aneurysm sac post-surgery. As a result, coiling has been coupled with stents to add structural rigidity over the neck of the aneurysm to prevent the coil from coming out of the sac. While this method is noninvasive, the small neck requirement dictates whether this method can be used.

1.3.3 Flow diverters

The newest method used to treat aneurysms is flow diverters (FDs). Flow diverters are a type of stent that differs in the degree of porosity. Stents have a long history of use in cardiac procedures and are essentially a tubular cage that opposes the blood vessel walls. Stents typically have a very low metal coverage, around 10%, and thus don't affect flow as much. Flow diverters, on the other hand, have 30-35% metal coverage. This is because FDs aim to change the blood flow profiles going into the aneurysm sac and help divert blood flow away from the sac. This reduces the amount of force the sac wall encounters and helps in healing the aneurysm. The current drawback of flow diverters is in the way they are currently fabricated. They are made by braiding wires into a cylindrical mesh. Densely meshed flow diverters could potentially present a problem when being deployed into the neurovasculature if arteries nearby become blocked by the flow diverter and risk being occluded. This is primarily the concern for small perforating arteries nearby the aneurysm sac which tend to be about 90-840 μms in diameter (Marinkovic et al. 1985).

In this project we base our model on the posterior circulation of the brain due to the large number of perforators found in that location and the reduced volumetric flow rates encountered. These two characteristics greatly increase the risk of occlusion and are likely

the reason why there are no current FDs approved for the posterior circulation region. FDs can also employ a similar endovascular technique for delivery used in coils and stents and thus are also a minimally-invasive approach that would not be limited by aneurysm morphology. The current deployment method for FDs follow the same initial steps as coiling. Once the guide has reached the aneurysm location, the FD that is currently in a sheath, can be deployed by unsheathing it. This project aims to characterize a new generation of FDs as well as optimizing the design to reduce the variability in flow changes due to the landing configuration of the device as well as not occluding perforators near the aneurysm sac. The current device that is being characterized was developed by one of our lab members, Ryan Peck, and uses a slightly different approach to deployment. The solid construct model that is described herein is mounted on a balloon at the end of the catheter that is then allowed to be expanded once it has reached the desired location.

2. METHODS

2.1 Device Fabrication

Micro-Electro-Mechanical System (MEMS) fabrication techniques allow for micron-scaled features of very high detailed designs to be fabricated. Well established techniques have been developed with silicon (Si) and have advanced due to the need in the computational sector. While silicon's electrical properties (e.g. low band gap) and ubiquity have driven previous fabrication research, it has many mechanical properties that preclude its use in implants (e.g. low fracture toughness). For these reasons, MEMS-based fabrication techniques have found little utility in the medical device sector. However, previous work in our lab has extended the capability for submicron-scale subtractive manufacturing to be utilized in Titanium. Titanium (Ti) has been greatly studied both for its strength and biocompatibility due to the native-oxide layer that forms on the surface of the metal. While various other materials have found use in traditional stent fabrication (e,g. NiTiNol, CoCr, SS) these materials have chemistries which introduce prohibitive complexity into the chemical-based material removal processes utilized in MEMS. Additionally, these chemistries have been shown to induce their own adverse biological responses (e.g. inflammation, nickel-sensitivity). Lastly, titanium's elastoplasticity allows for the accommodation of large strains without fracture. This enables the utilization of design concepts borrowed from traditional stents and minimizes the embolization risk associated with brittle fracture.

MEMS uses a combination of additive and subtractive manufacturing techniques in order to achieve the final design. Plasma-enhanced chemical vapor deposition (PECVD) is an additive step that allows for thin films to be deposited on surfaces from a gas state. In

order to create a template for the device, PECVD is used to deposit a thin film of SiO_2 onto the titanium substrate. A thin layer of photo resist is then spin-coated on top of the SiO_2 layer. The photo resist is then exposed to the mask pattern of the device under UV light in order to transfer the design into the resist by lysing the polymer chains in the exposed regions. Once the underlying SiO_2 hard mask is exposed after developing the photoresist, it can then be etched using a fluorine-based etch. This allows for the pattern of the photoresist to be transferred onto the SiO_2 layer. Now that the pattern is on the SiO_2, it can be etched onto the Ti substrate. HARFD fabrication requires etching all the way through the Ti film and is thus called a through etch. Once this final step is completed the device pattern has been etched into the Ti foil and can then be cleaned to remove the remaining SiO_2 or photoresist that was left on the surface of the device from the initial steps.

2.1.1 Device Fabrication Procedure

An 80 um thick commercially-pure (99.6% Ti, Tokyo Stainless Grinding Co.) Ti foil was cut into smaller sheets of 1.5 cm by 2 cm squares. The squares were then attached to a smaller piece of a silicon wafer for stability when moving the sample. The Ti was then put into the PECVD (ICP-PECVD, VLR Unaxis St. Petersburg, FL) and a 4.2 um layer of SiO_2 was deposited onto the foil. Once the SiO_2 has been deposited we spin-coated photoresist (AZnLOF 2070, Clariant, Muttenz, Switzerland) and used a positive mask to transfer the device patter onto the mask. The sample then underwent Si etching and Ti-through etching in order to transfer the pattern onto the SiO_2 and eventually etch through the Ti. A schematic of the fabrication process can be seen in Figure 2.

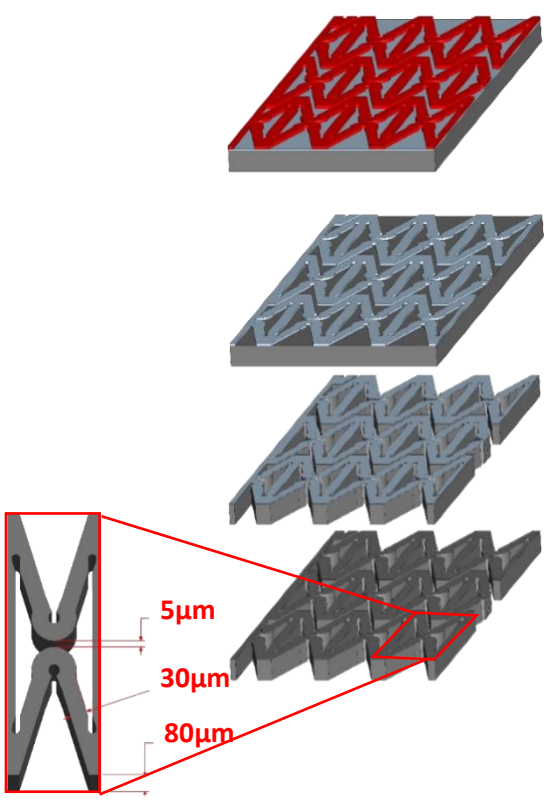

a) Photoresist exposed and developed on SiO_2/Ti Subtrate

b) PR removal, mask definition by F-Based dry etch

c) Mask Pattern Transfer by Ti DRIE (Deep-Reactive Ion Etching)

d) Residual SiO_2 removed by F-Based dry etch

Figure 2: (a) Illustrates the photoresist being exposed and transferring the pattern onto the SiO_2. (b) illustrates the mask being etched into the SiO_2 (c) illustrated the mask pattern being through etched the titanium substrate (d) illustrates the final pattern on the titanium after the residual SiO_2 has been removed**.**

2.2 Mock Aneurysm Fabrication

With the advancement of 3D printing, we can design neurovasculature with aneurysm models in different shapes and locations, or even use CT scans to obtain patient specific vascular geometry models. These models can then be cast in polydimethylsiloxane (PDMS), which is an optically-clear silicone elastomer. Printing these models in acrylonitrile butadiene styrene (ABS) is ideal because the models are easily dissolvable in acetone. After encasing a positive ABS model in PDMS, it can be dissolved out leaving a negative cavity of the model in the PDMS. These PDMS models can be cast from very complex vascular geometries that precisely reproduce the geometries of the computational domains that we can then image on our particle image velocimetry (PIV) set up. One of the first concerns that was encountered with making these geometries was how to keep them suspended in the PDMS. The second challenge was that even though 3D printing has high resolution capacities, the 3D models are still left with surface ridges due to the way they are printed. 3D printing is an additive manufacturing process in which the material is deposited down in layers. Once a layer is completed, the nozzle is raised slightly to start the second layer, and because of this, it creates micron-scale stepped features on curved surfaces. Because of the capacity of PDMS to capture micron-scale features, this artifact of the 3D printing has the ability to transfer through the casting process which can contribute to light refraction and scattering, thereby affecting image quality. By leaving the models in an acetone vapor bath, we were able to smooth out the print until no visible steps were left. We mounted the inlet and outlet onto the walls of the model that were used to serve as a mold container which allowed for the suspension of the vasculature. PDMS has

a refractive index of 1.4 which is also very similar to that of the mock blood mixture of glycerol and water (Yousif et al., 2011). This matching of refractive indices ensures optical accuracy. The result is a model with high optical-clarity as seen in Figure 3.

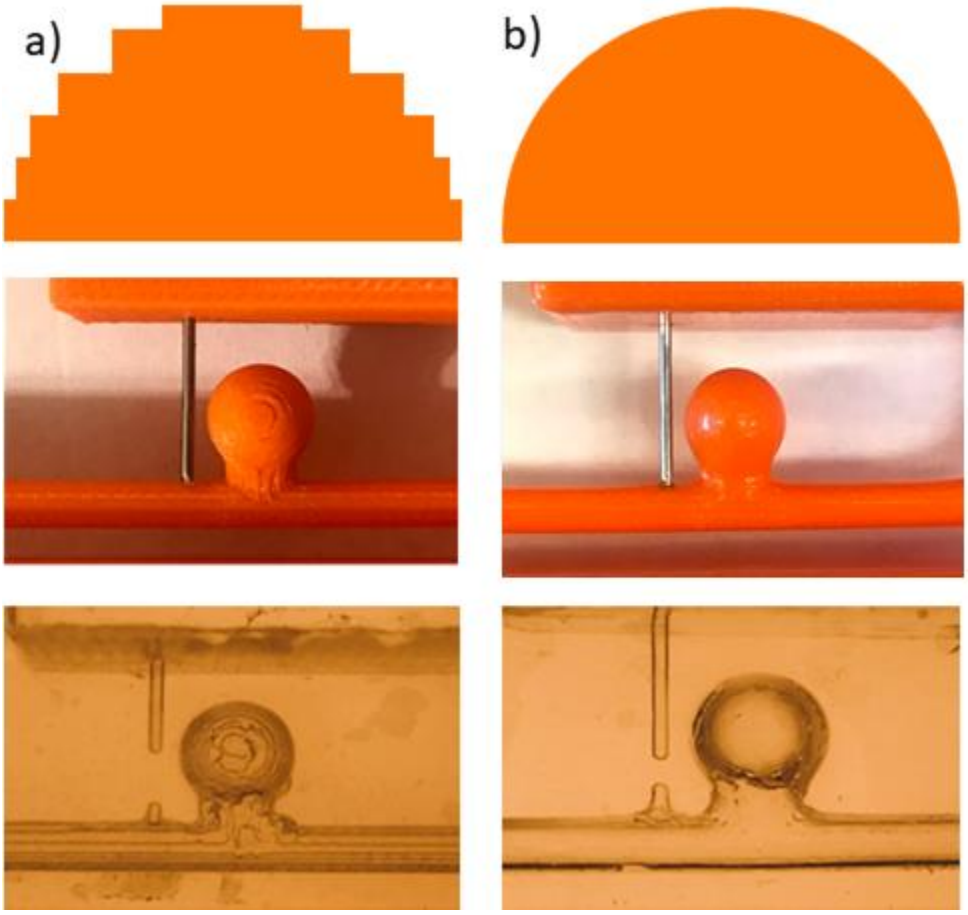

Figure 3: (a) From top to bottom illustrates the casting process and result with the step features on the 3D print, (b) from top to bottom illustrates the casting process and result with acetone vapor smoothing of the 3D print.

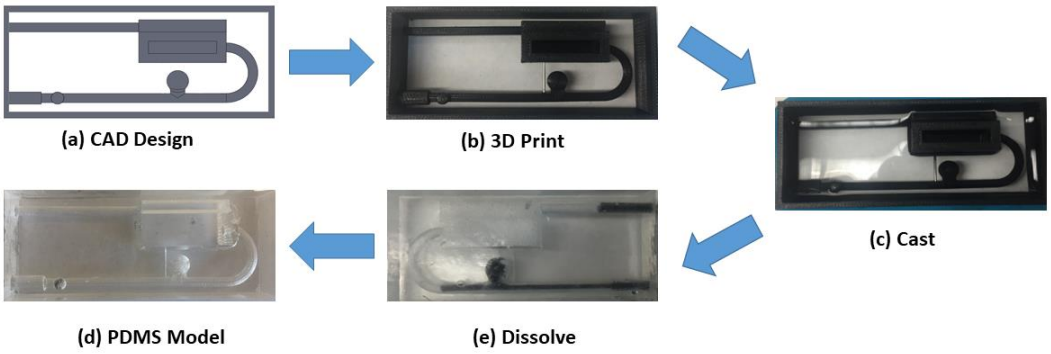

Figure 4: (a) Illustrates the CAD model, (b) shows the 3D printed model, (c) demonstrates the PDMS casting step, (e) shows the ABS being dissolved with acetone, and (d) shows the final PDMS model.

2.2.1 Mock Aneurysm Fabrication Procedure

A 3D model of an idealized aneurysm with an 820 μm perforator was designed in SolidWorks and printed on a Stratasys Dimension printer (Eden Prairie, Minnesota). The model was then placed into an acetone vapor smoothing chamber for an hour to smooth out the step features of the printer, thus leaving a smooth surface. The model was then fixed with putty onto a glass slide and a 10:1 mixture of PDMS-Monomer:Cross-linker was poured over the model into the mold. After a 24-hour curing period, the model was sonicated in acetone to dissolve the ABS, leaving a negative model of the 3D printed design. The model was then imaged under a microscope and ImageJ was used to verify the measurements of the models remained accurate. The features are shown in Figure 5. The parent artery was chosen to be 3 mm to mimic the average diameter seen in the basilar artery. The perforator was set to 820 μm which was chosen from the range of values of

perforators seen around the Circle of Willis, and the aneurysm was set to 6.5 mm (Marinkovic et al. 1985). Due to current limitations of the 3D printer resolution, the perforator could not be printed and instead a 26-gauge needle was used. The outer diameter of the needle matched the diameter of the perforator that was being modeled in SolidWorks.

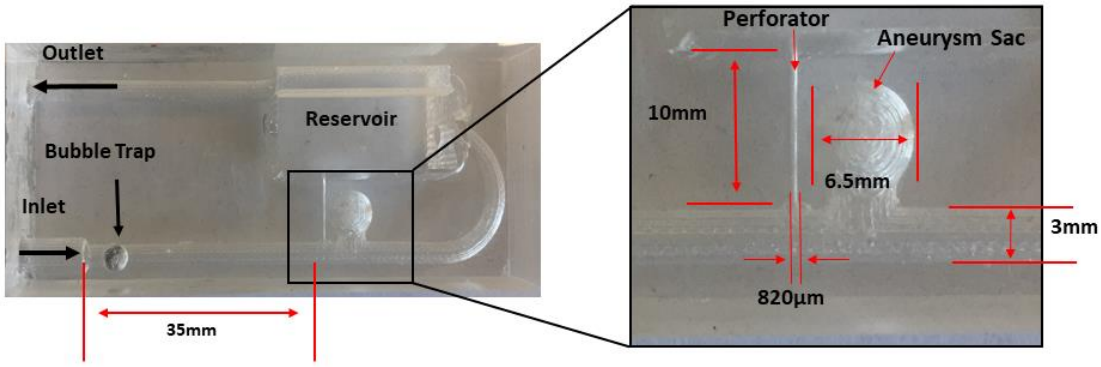

Figure 5: Detailed view of the PDMS model features and dimensions to mimic the posterior circulation anatomy.

2.3 Particle Image Velocimetry

Particle image velocimetry (PIV) is a flow visualization technique that is used to determine velocity fields in fluids. Using this technique, we observed and quantified the changes in flow in a mock aneurysm due to the presence of a flow diverter. PIV uses a laser to excite fluorescent particles and the light they emitted is captured by a high-speed camera as they move along a flow domain. The concentration of particles used to seed the flow domain should be high enough to capture the flow field but also small enough that the particles don't affect the flow characteristics trying to be observed. By knowing the sample rate at which the images are being taken at we can calculate the difference in time between

the images, Δt, -1500 Hz in this case. Time between the images is then calculated by using the inverse of the frequency which is 0.6 ms. An image of a known size is then captured to determine a scaling factor from units of the image into physical units (i.e. pixels/mm). In order to calculate the velocity of the fluid we can use the images captured on the PIV set up and calculate the displacement in the x direction, Δx. To calculate each local velocity vector, the entire image is split into smaller interrogation windows with about 5 particles per window. The displacement of each window can then be found by using a cross-correlation function between the particle intensity maps of image pairs. A schematic of the PIV set up is shown in Figure 6.

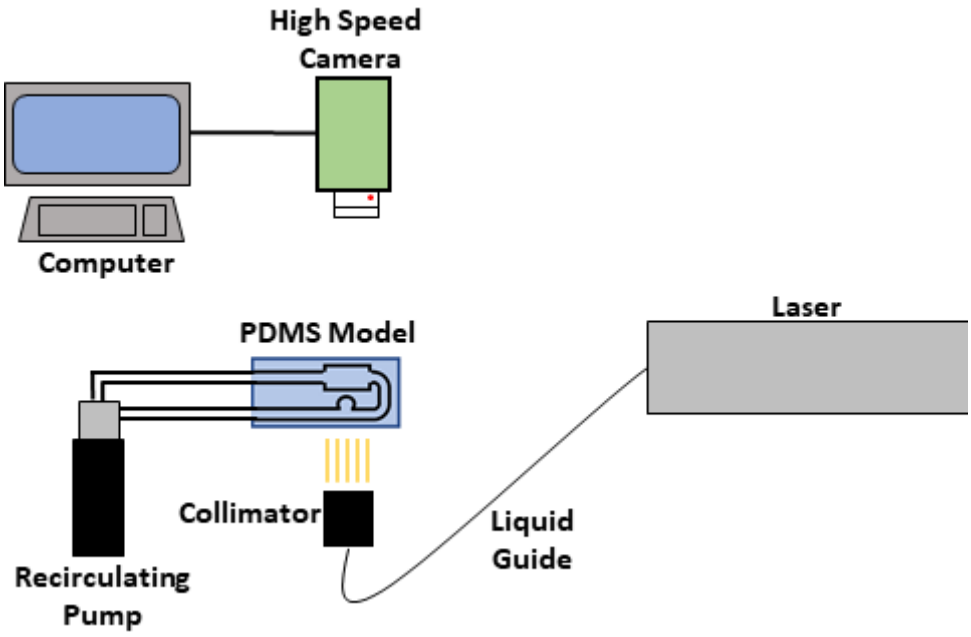

Figure 6: The main components for the PIV system include the laser, high-speed camera, collimator, PDMS model, and a desktop computer. The laser beam is diffused through the collimator and is used to illuminate the fluorescent particles flowing through the PDMS model. The camera captures images at 1500 Hz and transfers them to the computer for further analysis.

2.3.1 Particle Image Velocimetry Acquisition

A Micropump (GA Model, Micropump, Vancouver, WA) was set to a flow rate of 100 mL/min to match biological conditions seen in the neurovasculature and was attached to a PDMS mock model (Model 2, 3DMS, Riverside, CA) with a 3 mm internal diameter (ID) parent vessel to resemble the basilar artery, an 820 um ID perforator, and a 6 mm diameter saccular aneurysm with a 4.5 mm neck. This aneurysm geometry was chosen to represent a dome-to-neck ratio for which coiling is contraindicated, and to mimic a posterior circulation aneurysm with a perforator at risk of occlusion if treated with current FDs. In order to mimic the density and viscosity of blood, a 60:40 mixture of Water to Glycerol was used. The mixture was seeded with a 2% by volume concentration of 10.3 um fluorescent microspheres (PSF-010UM, Magsphere, Pasadena, CA) with a maximum emission wavelength of 501 nm. A Litron laser (Dantec, United Kingdom) with an excitation wavelength 527 nm was used to excite the fluorescent particles. The fluid was imaged using a highspeed camera (SpeedSense VEO 640 (Vision Research), Dantec, United Kingdom) at 0.65X magnification for the aneurysm sac, and at 1.55X in the perforator artery with a resolution of 2560x1600 pixels and recorded at 1500 fps. We captured video for 750 frames which totals half a second of flow through the model. Using Dynamic Studios Software (Dantec, United Kingdom), background correction was performed by subtracting the temporal image mean from each frame as shown in Figure 7. Interrogation window sizes were empirically determined based on the expected velocities encountered in each region of interest (ROI).

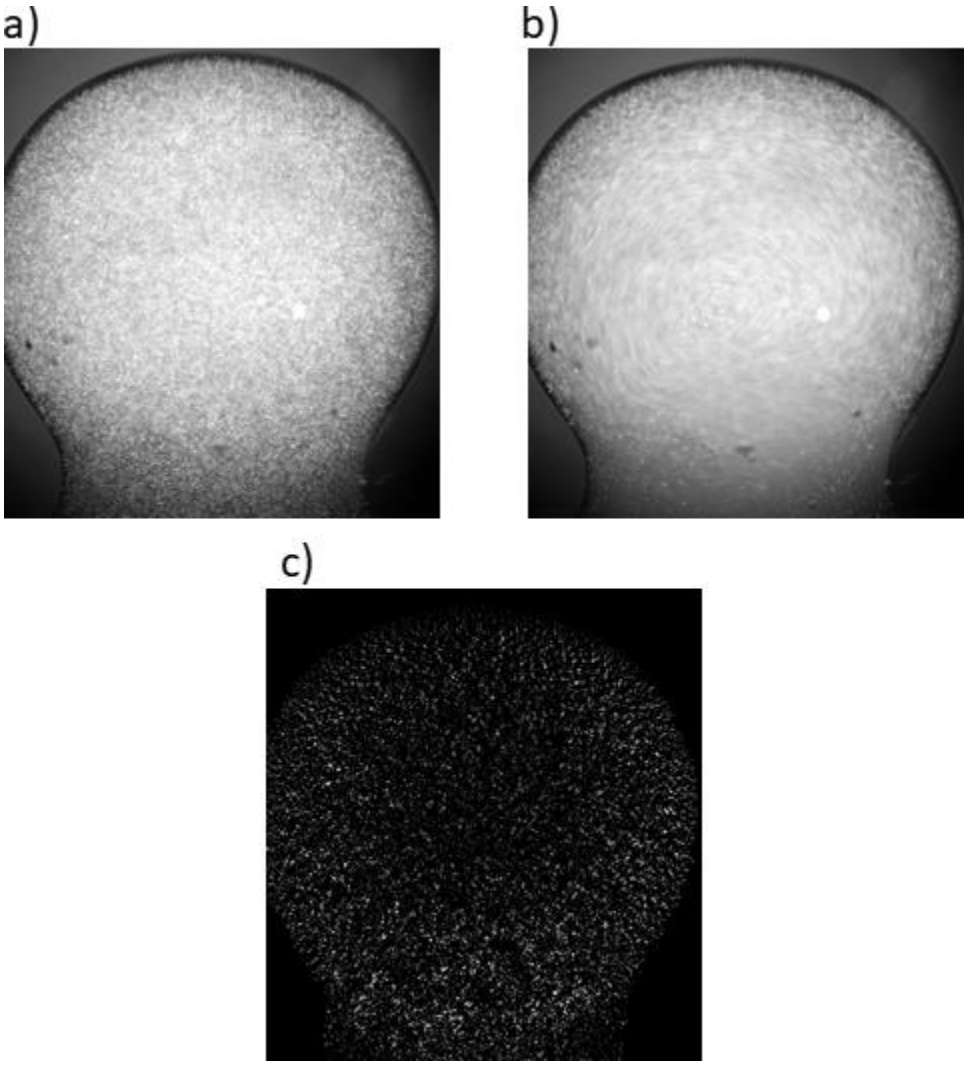

Figure 7: (a) The raw image, taken with a flow rate of 100 mL/min, seeded with a 2% bead density, and imaged at 1500 Hz, (b) the averaged image over the 750 images collected, (c) post-processed image after subtracting (b) from (a).

2.4 Computational Modeling

In order to obtain a greater understanding of the flow interaction, computational fluid dynamics (CFD) can be used to simulate fluid flows. CFD was used after PIV validated the initial CFD results and was used to predict flow profiles for different aspect ratio (AR) devices in order to find an optimal design. ANSYS FLUENT (Canonsburg, PA)

was used to carry out the CFD portion of this work. For CFD simulations the steps can be broken down into pre-processing, results, and post-processing. Pre-processing entails designing the desire geometry; in our case, a mock aneurysm model with the parent, perforator, and aneurysm details taken from literature values from the basilar section of the brain vasculature. Additionally, pre-processing requires an indication of regions of the geometry where boundary conditions will be applied. In this specific geometry this is accomplished by labeling the inlet and outlet. The results will allow for vector maps to be generated and further analyze how the flow is behaving with the FD deployed.

2.4.1 Computational Fluid Dynamics Simulation

In order to match the PIV setup, the fluid motion condition and parameters were classified in the following ways for ANSYS FLUENT. The properties of blood that were input into FLUENT were regarded as steady-state, it was classified as a Newtonian fluid, the fluid was considered incompressible in which the density is not a function of space and time, the continuity equation is satisfied, and the effects due to gravity were ignored. In order for it to be streamlined it had an entrance length of 35 mm to allow the flow to fully develop before interacting with the perforator and the aneurysm. The two governing equations used were the Navier-Stokes equations and the continuity equation, which are listed below.

The Navier-Stokes equation: $\rho[\frac{\partial \vec{v}}{\partial t} + (\vec{v} \cdot \nabla)\vec{v})] = -\nabla P + \mu \nabla^2 \vec{v}$

and the continuity equation: $\nabla \cdot v = 0$

The governing equations were input into the simulation as well as a no-slip boundary condition at the walls. Flows in the basilar artery have been reported to vary between 80 to 120 mL/min due to the variations in the Circle of Willis (Bogren et al. 1994). With a chosen flow rate of 100 mL/min, and the cross-sectional area of out parent artery, the inlet velocity of 0.235 m/s was applied with both perforator outlet as well as the parent outlet set to atmosphere. A blood viscosity (μ) of 4.7 cP and a density (ρ) of 1000 kg/m^3 taken from literature values was used to define the properties of the fluid in ANSYS (Letcher et al. 1981).

3. Results

3.1 Introduction

Traditional flow diversion devices are of a braided construct which have smaller unit cells which repeat more frequently than our HARFD design. Because of the heterogeneity of the HARFD, it was postulated that this device may be more sensitive to placement within the artery. In order to evaluate this sensitivity, the HARFD was deployed in 4 different locations to encompass the best (no perforator obstruction), worst (strut landing in the center of perforator opening), and nominal cases (50% strut obstruction of the perforator opening) for deployment. Best case deployment is when the device lands with an open perforator configuration. This places no struts under the perforator, thus allowing for the most unobstructed flow profile into the perforating artery. Worst case deployment is considered to be when there is a strut that lands directly underneath the perforating artery. The two middle cases are when half of the strut lands at the leading edge of the perforator or at the trailing end of the perforator. In each of these cases the placement and number of struts that cover the neck of the aneurysm sac change as a result of landing different configurations under the perforator. The configuration can be seen in Figure 8. Current-generation FDs differ in possible porosity due to their braided mesh design. It has been reported that one can get a range of 26% to 60% porosity due to how much compression is applied to the device when deployed (Shapiro et al. 2014). The results are presented in a "percent reduction" of flow from the unstented case. The spatial velocity magnitude was calculated in two regions of interest (ROI), the aneurysm sac and the perforator, to observe the effects of HARFD. The calculations are listed below for reference:

Spatial Velocity Average: $\bar{v} = \frac{1}{A}\int \int_{ROI} |v| \, dx \, dy$

Percent reduction in Velocity: $\% \, Reduction = \frac{v_{in} - v_f}{v_{in}} \; X \; 100$

Where v_{in} is the initial velocity recorded, and v_f is the velocity recorded post deployment of the FD.

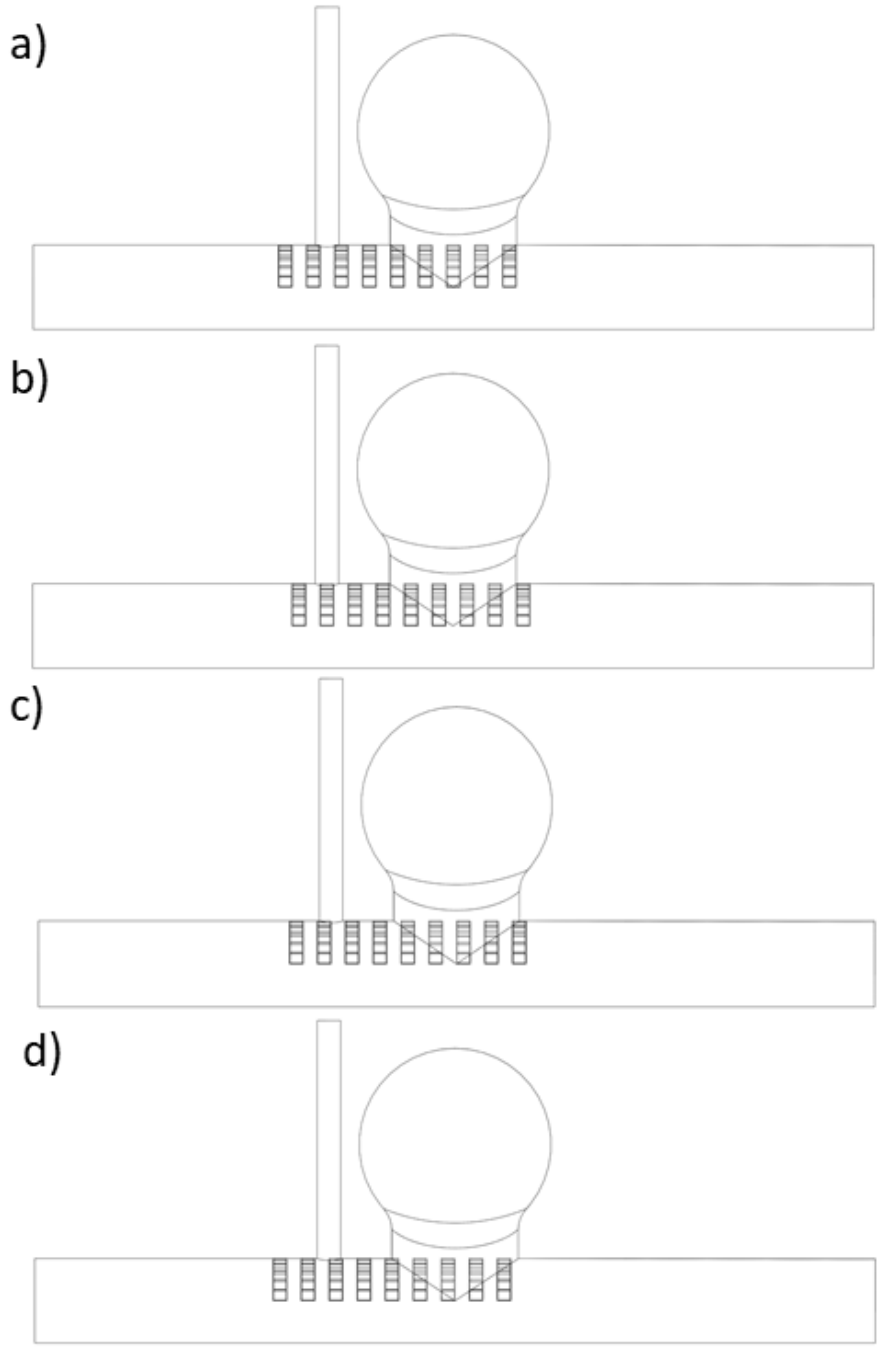

Figure 8: Strut landing configurations: (a) Best case with an open perforator configuration, (b) worst case with a closed perforator configuration., (c) leading edge case, (d) trailing edge case.

3.2 Particle Image Velocimetry Results

3.2.1 Perforator

Over the 4 different cases seen in perforator landing, the difference between flow reduction between the best case and worst-case landing was only 15%. In total, the difference between an unstented and the worst case is 10.8% in flow reduction. The two middle cases reduced flow by 5.67% and 3.37% respectively between leading and trailing cases. Compared to other literature values, there are some reports of up to 60% flow reduction in the perforators (Roszelle et al. 2013). Figure 9 shows the percent flow reductions while Figure 10 shows the flow profiles.

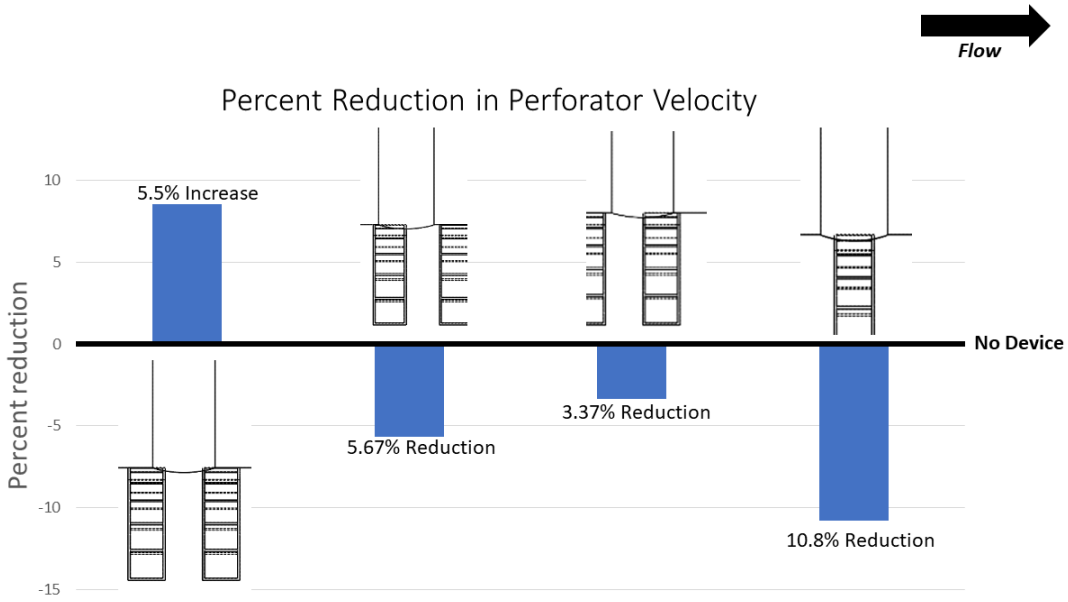

Figure 9: In the open perforator placement case, we observed a 5.5% increase, in the leading edge we observed a 5.67% reduction, in the trailing edge we observed a 3.37% reduction, and in the closed perforator case we observed a 10.8% reduction.

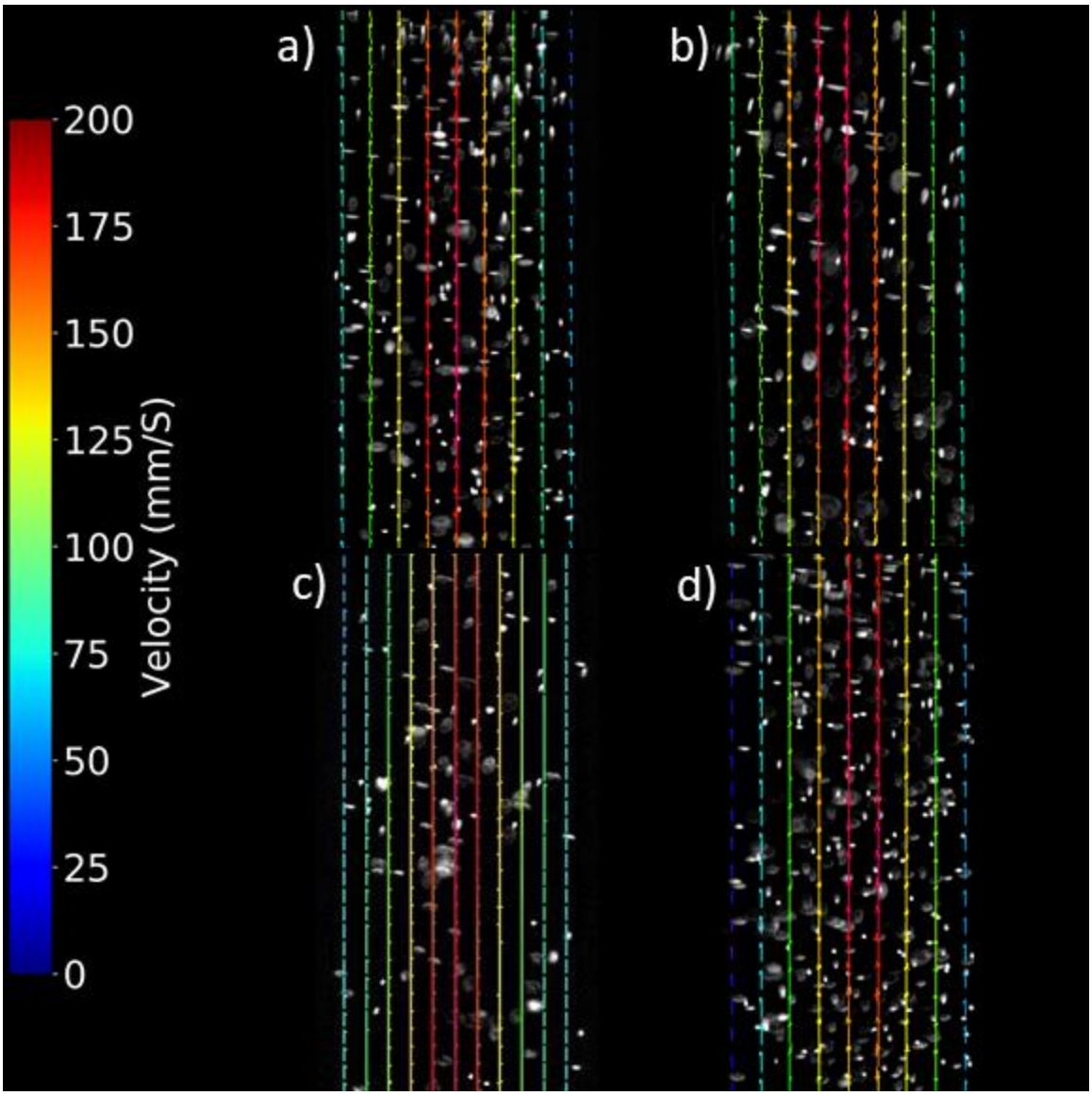

Figure 10 : Flow profiles in the perforator: (a) best case, with no strut under the perforator, (b) leading edge case, where the strut covers the front end of the perforator, (c) trailing edge case, where the strut covers the end of the perforator, (d) worst case, where a strut lands in the center of the perforator. The range of changes experienced by the perforator was +5.5% (best case) to -10.8% (worst case) reduction.

3.2.2 Aneurysm Sac

Average velocity reduction in the aneurysm sac was consistent across all four placements with a range from 84% to 87% in flow velocity which is shown in Figure 11. Flow realignment can be observed qualitatively by the changes in the flow profiles seen in Figure 12. In the unstented case, a large in-jet at the distal end of the aneurysm neck can be seen to go into the aneurysm sac and recirculated in the sac. However, in the HARFD case, we can see a realignment of the flow where velocity vectors largely remain parallel to flow in the parent artery. This realignment of flow is characteristic of treatment with current-gen FDs and has been remarked upon by other groups (Bouillot et al. 2014). This shift in flow field morphology can be attributed to the presence of stent struts in the aneurysm neck, which disrupt the ability for the high-velocity parent arterial flow to drive circulation in the aneurysm sac by the transmission of shear. Thusly, the magnitude of intra-aneurysmal velocity is reduced and the remaining dominant forces acting on the fluid are a result of the pressure differential along the parent artery. This shift in regimes has been shown to be the cause of this realignment of flow, which is a characteristic successful FD treatment (Kulcsár et al. 2012)

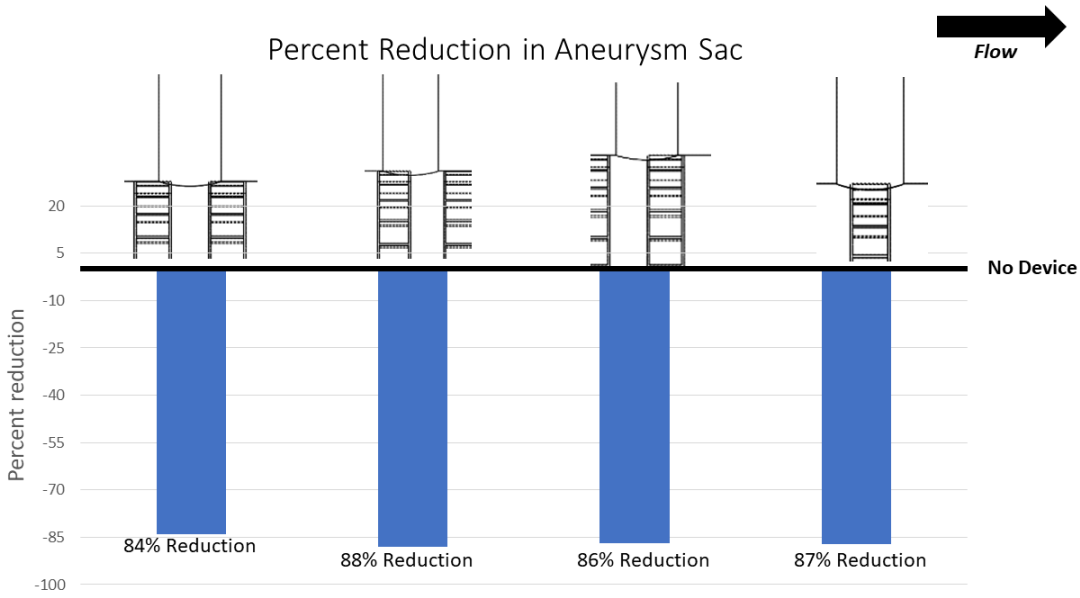

Figure 11: In the open perforator placement case we observed an 84% reduction, in the leading edge we observed an 88% reduction, in the trailing edge we observed an 86% reduction, and in the closed perforator case we observed an 87% reduction.

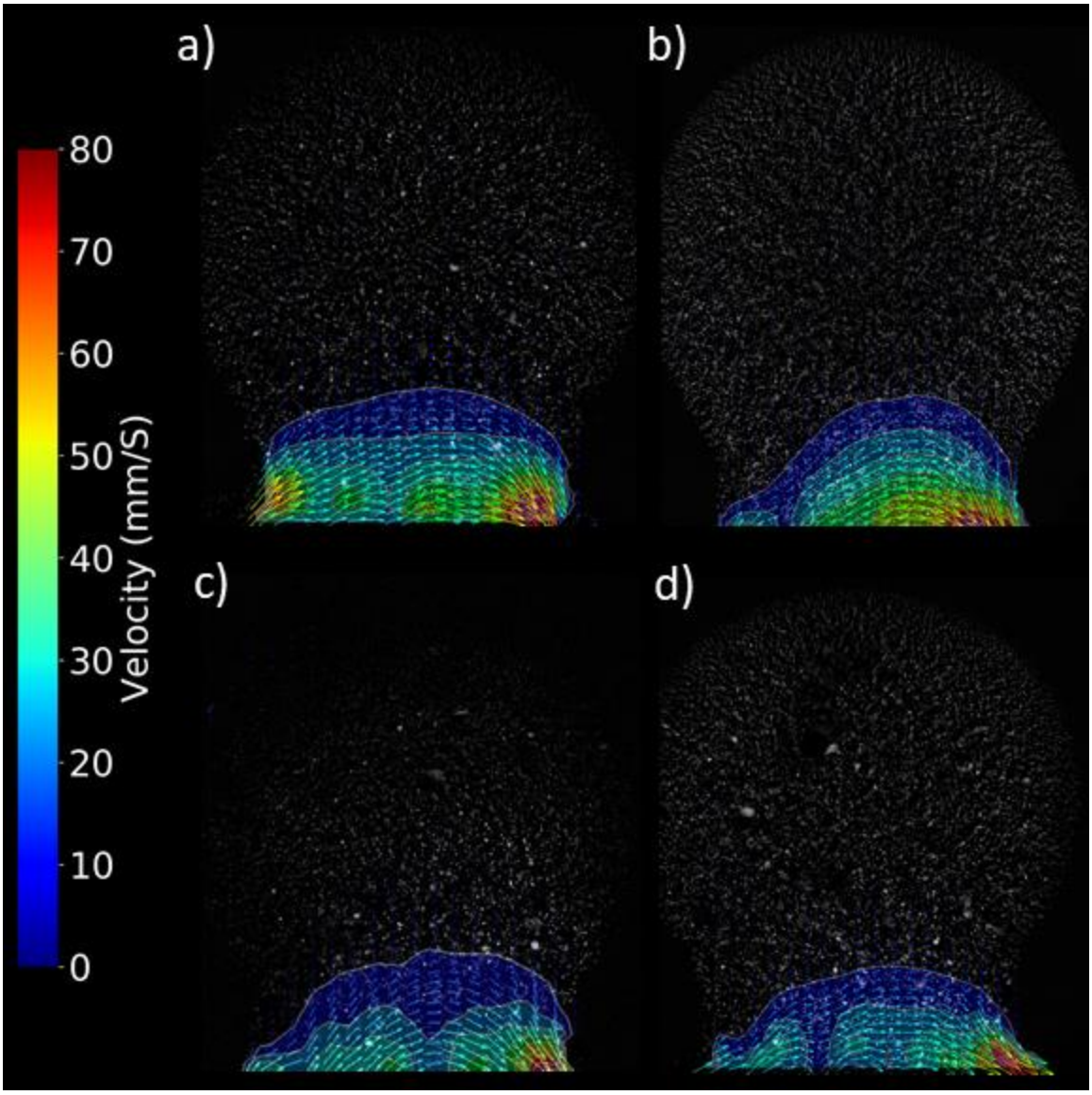

Figure 12: Flow profiles in the aneurysm sac: (a) best case, with no strut under the perforator, (b) leading edge case, where the strut covers the front half of the perforator, (c) trailing edge case, where the strut covers the back half of the perforator, (d) worst case, where a strut lands in the center of the perforator. The flow diverter causes a realignment of flow in the neck area of the aneurysm sac.

3.3 Computational Fluid Dynamic Results

The results of the CFD for the worst-case placement (closed perforator configuration) showed that by changing the AR of the device affected the flow reduction in the perforator, but still exhibited similar flow reduction in the sac. The study included struts of 15 μm, 30 μm, 50 μm, and 150 μm in height while maintaining the same width of 30 μm. The percent reduction in velocity in the perforator was the least with the 15 μm thick struts and only reduced flow by 6.7% while the 150 μm struts reduced it by 14.5%. The reductions seen in the sac varied from 70% reduction with the 15 μm thick struts, at 30 μm 80% reduction was observed, 50 μm reduced flow by 82%, and 150μm only reduced velocity by 76%. The reductions in perforator velocity and aneurysm sac velocity can be seen in Figure 13 and 14, respectively.

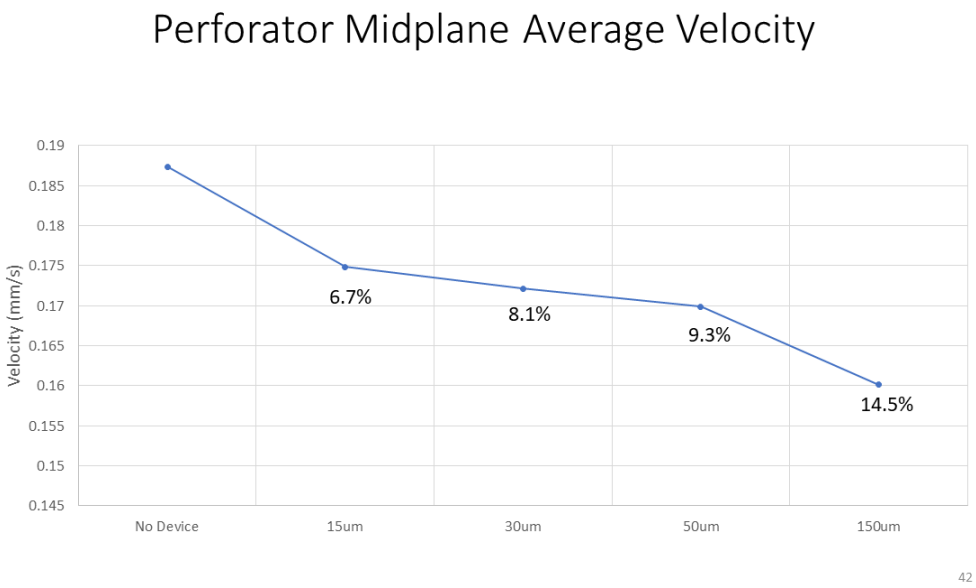

Figure 13: Velocity reductions in the perforator with respect to a change in strut height. As the struts become thinner, the perforator experiences less flow reductions**.** The current device has 80 μm thick struts and reduced flow by 10.8% in the closed perforator configuration, while running the PIV experiments.

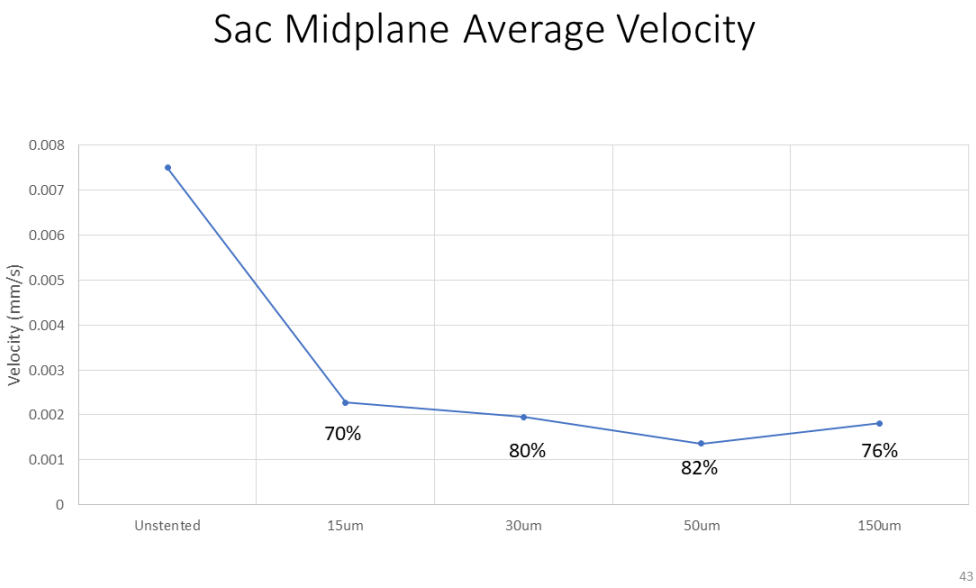

Figure 14: Velocity reductions in the aneurysm sac with respect to a change in strut height. The reduction in flow velocities vary between 70% and 82%. The current device has 80 μm thick struts and reduced flow by 87% in the closed perforator configuration, while running the PIV experiments.

4. Conclusion

4.1 Particle Image Velocimetry

Flow profiles could be qualitatively seen to change after deployment of the flow diverter. The flow reduction caused by HARFD in the aneurysm sac were not affected by the placement of the device since they showed an 86% average flow reduction. The flow reduction in the perforator varied between +5.5% to -10.8% for the best vs worst case placement. We observed a reduction between 16% to 41% between our PED placement which had a variation in porosity between 56% to 76% porous Compared to current flow diverters, the ranges are within a smaller window of variation indicating that when deployed, the HARFD always reduced flow into the perforator less than PED. This is important as surgeons have indicated that there is very little visibility when deploying the current FDs during procedures and there is little control of porosity. The current woven design of current flow diverters allows for large variability in unit cell geometry due to the ability for wires to slide past each other. This enables the device to accommodate varying arterial diameters but also may lead to changing porosity though the device. With HARFD, that possibility is no longer a concern due to the nature of the fabrication process which allows struts to be monolithically integrated into a solid construct. The concerning issue with a strut landing under the perforator was seen to have negligible effect; only reducing flow in the perforator by a maximum of 12% while reports have indicated up to 60% flow reduction when using PED.

4.2 Computational Fluid Dynamics

This project explored the effect of the aspect ratio (AR) of the device on intra-aneurysmal and perforating-artery flows. The sensitivity study indicated that lower AR devices induced 6.7% decrease in flow change into the perforator while still maintaining a 70% reduction in the aneurysm sac. This allows for further reduction in variability in the perforator that then translates to placement being less sensitive for deploying HARFD. In contrast, commercially available devices have an AR of 1 due to the height and the width of the wire being the same. This is likely the reason it has been reported that more than one PED can be placed during surgery (Miyachi et al. 2018). It was also noted that when increasing the thickness of the device, the reduction in velocity in the perforator was 14.5% and in the aneurysm, sac was 76%. At 80 μm thick struts we observed an average reduction of 86.33% in the sac, but at 150 μm the reduction was only 76%.

4.3 Limitations

Although steady state, Newtonian flow is not encountered in the neurovasculature, it is well studied in the literature that these parameters help in observing the maximum values of velocity that would be seen at the peak of the pulsatile flow (Milnor 1989). Pulsatile flow as well as non-Newtonian parameters would need to be implemented into both models in order to observe and study more complex transient behavior. However, a simplified aneurysm model was used to gather the information of how a FD affects the flow post deployment. While it does help to provide insight into the flow characteristics of the aneurysm sac, the actual neurovascular geometry can vary as stated with asymmetrical

Circle of Willis. Creating a wide array of patient models would allow for further investigation on how the FD will affect different aneurysm geometries, as well as different configurations of Circle of Willis vasculature.

4.4 Future work

Fabrication of a HARFD with a thinner Ti foil at 50 μm was attempted based on the results of the optimization study from the CFD. However, the current etch recipe was too aggressive for the thinner foil and resulted in undercutting the walls of the device. Further investigation would need to be done into varying the etch parameters to complete device fabrication with a thinner Ti foil. Finite element analysis should also be conducted to see if the residual stress that the cross beams exhibit when expanding can withstand deployment or if deployment would break the beams. Sizes of the struts can also be examined to see if increasing their size would allow for more space in the unit cell and allow more flow to pass through the struts. By increasing the openings in the struts, it is possible that more flow will pass in between struts and the amount of reduction seen in the perforator might decrease more. However, it is also possible that this would allow for greater flow into the aneurysm sac. While this device allows for the utilization of mechanisms (i.e. aspect-ratio) that decrease sensitivity to this tradeoff, the optimal configuration of porosity and aspect ratio remains to be seen.

New studies have started to flow whole blood through their mock aneurysm setups to explore clot formation caused by FDs (Gester et al. 2016). It was shown that no blood clot was developed in the model when the FD wasn't present. However, after a 5-hour flow

period, traces of fibrin network started to form with a FD present. After 12 hours a clot was present in the aneurysm. By conduction a similar experiment, we would want to explore if HARFD has a different time range for the formation of clots, but also observe if the perforator artery becomes occluded.

5. Bibliography

Benjamin, Emelia J., Paul Muntner, and Márcio Sommer Bittencourt. "Heart disease and stroke statistics 2019 update: a report from the American Heart Association." *Circulation* 139.10 (2019): e56 e528.

Bogren, Hugo G., Michael H. Buonocore, and Wei-Zhong Gu. "Carotid and vertebral artery blood flow in left-and right-handed healthy subjects measured with MR velocity mapping." *Journal of Magnetic Resonance Imaging* 4.1 (1994): 37-42.

Bouillot, Pierre, et al. "Particle imaging velocimetry evaluation of intracranial stents in sidewall aneurysm: hemodynamic transition related to the stent design." *PLoS One* 9.12 (2014): e113762.

Clauser, Johanna, et al. "A novel plasma-based fluid for particle image velocimetry (PIV): In-vitro feasibility study of flow diverter effects in aneurysm Model." *Annals of biomedical engineering* 46.6 (2018): 841-848.

Dandy, Walter E. "Intracranial aneurysm of the internal carotid artery: cured by operation." *Annals of surgery* 107.5 (1938): 654.

Demaerschalk, Bart M., Ha-Mill Hwang, and Grace Leung. "US cost burden of ischemic stroke: a systematic literature review." *The American journal of managed care* 16.7 (2010): 525 533.Keedy, Alexander. "An overview of intracranial aneurysms." *McGill Journal of Medicine: MJM* 9.2 (2006): 141.

Gester, K., et al. "In vitro evaluation of intra-aneurysmal, flow-diverter-induced thrombus formation: a feasibility study." *American Journal of Neuroradiology* 37.3 (2016): 490-496.

Keedy, Alexander. "An overview of intracranial aneurysms." *McGill Journal of Medicine: MJM* 9.2 (2006): 141.

Kulcsár, Zsolt, et al. "Flow diversion treatment: intra-aneurismal blood flow velocity and WSS reduction are parameters to predict aneurysm thrombosis." *Acta neurochirurgica* 154.10 (2012): 1827-1834.

Letcher, Robert L., et al. "Direct relationship between blood pressure and blood viscosity in normal and hypertensive subjects: role of fibrinogen and concentration." *The American journal of medicine* 70.6 (1981): 1195-1202.

Marinkovic, S. V., et al. "Perforating branches of the middle cerebral artery. Microanatomy and clinical significance of their intracerebral segments." *Stroke* 16.6 (1985): 1022-1029.

Milnor, W. R. "Hemodynamics, 1989." *Baltimore, MD: Williams and Wilkins*.

Miyachi, Shigeru, et al. "Tied Pipeline: A Case of Rare Complication." *Neurologia medico-chirurgica* (2018): cr-2017.

Novakovic, Roberta, G. Toth, and P. D. Purdy. "Review of current and emerging therapies in acute ischemic stroke." *Journal of neurointerventional surgery* 1.1 (2009): 13-26.

Peck, Ryan A., et al. "Meso-scale particle image velocimetry studies of neurovascular flows in vitro." *JoVE (Journal of Visualized Experiments)* 142 (2018): e58902.

Roszelle, Breigh Nonte, et al. "In vitro and in silico study of intracranial stent treatments for cerebral aneurysms: effects on perforating vessel flows." *Journal of neurointerventional surgery* 5.4 (2013): 354-360.

Shapiro, M., et al. "Variable porosity of the pipeline embolization device in straight and curved vessels: a guide for optimal deployment strategy." *American Journal of Neuroradiology* 35.4 (2014): 727-733.

Stojanović, Nebojša, et al. "Presence of anatomical variations of the circle of Willis in patients undergoing surgical treatment for ruptured intracranial aneurysms." *Vojnosanitetski pregled* 66.9 (2009): 711-717.

Van Rooij, W. J., and M. Sluzewski. "Perforator infarction after placement of a pipeline flow-diverting stent for an unruptured A1 aneurysm." *American Journal of Neuroradiology* 31.4 (2010): E43-E44.

Wang, Cheng-Bin, et al. "Flow diverter treatment of posterior circulation aneurysms. A meta-analysis." *Neuroradiology* 58.4 (2016): 391-400.

Yousif, Majid Y., David W. Holdsworth, and Tamie L. Poepping. "A blood-mimicking fluid for particle image velocimetry with silicone vascular models." *Experiments in fluids* 50.3 (2011): 769-774.